Supramolecular Stabilization of Metastable Tautomers in Solution and the Solid State

ARTICLE *in* CHEMISTRY - A EUROPEAN JOURNAL · DECEMBER 2014

Impact Factor: 5.73 · DOI: 10.1002/chem.201403543

9 AUTHORS, INCLUDING:

Marina Juribašić
Ruđer Bošković Institute
20 PUBLICATIONS **164** CITATIONS
SEE PROFILE

Nikola Bregovic
University of Zagreb
13 PUBLICATIONS **54** CITATIONS
SEE PROFILE

Vladislav Tomišić
University of Zagreb
49 PUBLICATIONS **376** CITATIONS
SEE PROFILE

Marina Cindrić
University of Zagreb
107 PUBLICATIONS **886** CITATIONS
SEE PROFILE

ChemPubSoc Europe

DOI: 10.1002/chem.201403543

CHEMISTRY
A European Journal
Full Paper

Tautomerism

Supramolecular Stabilization of Metastable Tautomers in Solution and the Solid State

Marina Juribašić,[a] Nikola Bregović,[b] Vladimir Stilinović,[b] Vladislav Tomišić,[b] Marina Cindrić,[b] Primož Šket,[c, d] Janez Plavec,[c, d, e] Mirta Rubčić,[b] and Krunoslav Užarević*[a, b]

Abstract: This work presents a successful application of a recently reported supramolecular strategy for stabilization of metastable tautomers in cocrystals to monocomponent, non-heterocyclic, tautomeric solids. Quantum-chemical computations and solution studies show that the investigated Schiff base molecule, derived from 3-methoxysalicylaldehyde and 2-amino-3-hydroxypyridine (**ap**), is far more stable as the enol tautomer. In the solid state, however, in all three obtained polymorphic forms it exists solely as the keto tautomer, in each case stabilized by an unexpected hydrogen-bonding pattern. Computations have shown that hydrogen bonding of the investigated Schiff base with suitable molecules shifts the tautomeric equilibrium to the less stable keto form. The extremes to which supramolecular stabilization can lead are demonstrated by the two polymorphs of molecular complexes of the Schiff base with **ap**. The molecules of both constituents of molecular complexes are present as metastable tautomers (keto anion and protonated pyridine, respectively), which stabilize each other through a very strong hydrogen bond. All the obtained solid forms proved stable in various solid-state and solvent-mediated methods used to establish their relative thermodynamic stabilities and possible interconversion conditions.

Introduction

Control over the occurrence of a target tautomer in the condensed state has attracted the broad attention of scientists from a fundamental point of view,[1] but it is also widely studied for the development of different functional systems, such as molecular machines and switches,[2] chemical information management systems,[3] and a new generation of pharmaceutics.[4] Unlike in solution, in which the equilibrium between different tautomeric forms can be manipulated by adjusting the medium properties (e.g., solvent polarity and proticity, pH),[5] in the solid state tautomeric compounds are usually present exclusively in one form. In more than 99% of the crystals of tautomeric compounds, the form present in the solid state represent the most stable tautomer, as calculated for the gaseous phase and/or observed in solution.[6] Rare examples for which more than a single solid tautomer emerges usually include stoichiometric[7] or nonstoichiometric[8] mixtures in the same crystal or as subunits of a single molecule existing as different tautomeric forms.[9] Also, the occurrence of tautomers as distinct crystalline forms (desmotropy) has been observed, though extremely rarely.[10,11] Although such structures that carry information on the supramolecular forces that stabilize each respective tautomer in the solid state do exist, and have proven helpful in bettering the tools for prediction and synthesis of materials containing the metastable tautomer in the solid state, this remains an undeveloped field of crystal engineering.[12] The manipulation with the target tautomeric forms in the solid state is far from a resolved issue.

A promising strategy for obtaining the less stable tautomers in the crystalline state was reported recently.[13] It relies on the premise that each tautomer has a specific potential for forming intermolecular bonds with surrounding molecules, thus resulting in specific supramolecular surroundings.[14,15] Cruz-Cabeza and co-workers have recently shown that in multicomponent solids (cocrystals), the proper choice of a cocrystal coformer can tune the interactions between the molecule and its sur-

[a] Dr. M. Juribašić,[+] Dr. K. Užarević
Ruđer Bošković Institute
Bijenička 54, Zagreb (Croatia)
Fax: (+385) 1-4680-245
E-mail: krunoslav.uzarevic@irb.hr

[b] N. Bregović,[+] Dr. V. Stilinović, Prof. V. Tomišić, Prof. M. Cindrić, Dr. M. Rubčić, Dr. K. Užarević
Department of Chemistry, Faculty of Science
University of Zagreb
Horvatovac 102a, Zagreb (Croatia)

[c] Dr. P. Šket, Prof. J. Plavec
Slovenian NMR Center, National Institute of Chemistry
Hajdrihova 19, Ljubljana (Slovenia)

[d] Dr. P. Šket, Prof. J. Plavec
EN-FIST Center of Excellence
Trg OF 13, 1000 Ljubljana (Slovenia)

[e] Prof. J. Plavec
Faculty of Chemistry and Chemical Technology, Physical Chemistry
University of Ljubljana
Aškerčeva 5, Ljubljana (Slovenia)

[+] These authors contributed equally to this work.

Supporting information for this article is available on the WWW under http://dx.doi.org/10.1002/chem.201403543.

roundings and thus compensate for the molecule's inherent instability. Although it is hard to control the way a compound will crystallize, cocrystallization with suitable coformers that bind specifically to the desired tautomeric form could lead to the stabilization of that particular form. The authors used computational methods to designate the most likely aggregation modes for each tautomer of their studied heterocycle. Based on the results, they have chosen suitable coformers and have successfully used this rational approach to isolate cocrystals containing both tautomeric forms of the heterocycle. This strategy not only allowed for isolating unstable tautomers as constituents of multicomponent solids, but also pointed to the possibility of achieving the same goal in monocomponent ones.[16] That can be accomplished by preparing such derivatives of the desired molecule or by tuning the reaction conditions[17] in which the molecules of the metastable tautomer are self-complementary, that is, a supramolecular stabilization in the crystal will be possible for the unstable, but not for the stable, tautomer.

As part of our research into coordination compounds, we have synthesized and investigated different tautomeric forms of imine ligands.[18] Recently we reported the first desmotrope of a Schiff base **1** (Scheme 1).[11] This salicylidene-based compound, in which each solid tautomer was also present in two additional polymorphic phases, served as a unique platform for the investigation of the phenomena related to solid-state proton transfer as well as tautomer and polymorph transformation. The larger stability of the enol tautomer, indicated by calculations and demonstrated by its predominance in solution, was also mirrored in the solid state: the two enol polymorphs were more stable than the ketone ones. These results were in compliance with the literature data, which predominantly stated that in salicylidene derivatives the enol was more stable,[19] although the tautomeric equilibrium could be affected by introduction of different substituents on either ring of the Schiff base.[20,21] The tautomerism in Schiff bases has been widely studied by experimental and computational methods due to related important macroscopic properties, such as thermochromism[22] or photochromism[23] and their potential applicability in sensing devices. However, the exact reason why a particular derivative occurs in the keto or the enol tautomeric form has not been definitely established and the knowledge is still related to case studies.

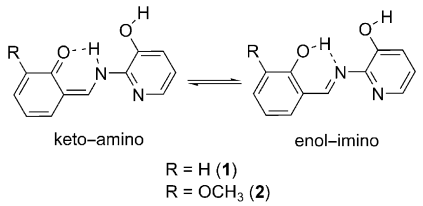

Scheme 1. Keto–enol tautomers of **1** and **2**.

The aim of the present study was to examine the prospect of modulating the stability order of tautomers established for **1**, both in the solid state and in solution, by introducing an electron-rich functionality, that is, a methoxy group, in the vicinity of its salicylidene oxygen atom (Scheme 1). Molecule **2** proved to be an extraordinary tridentate ligand in the synthesis of mechanosensitive coordination compounds.[24]

In solution, such modification induces a slight shift of the tautomeric equilibrium to an extent that depended on the solvent properties, whereas the inversion of the stability order was readily achieved in the solid state. In connection with this, we present herein a solid-state and solution study of altogether five solid forms of **2** exclusively in its keto–amino form. Three of these are polymorphs of **2**, and two of them correspond to the polymorphs of the molecular complex containing **2** and 2-amino-3-hydroxypyridine (**ap**). Importantly, even though the enol–imino tautomer of **2** is shown to be more stable both by quantum-chemical computations and by solution studies that combined several different approaches, the distinctive solid phases comprise only its metastable tautomer. This highlights, and allows for a thorough discussion of, the decisive role of supramolecular interactions in the stabilization of metastable species in the solid state. The extremes to which this can lead are best depicted by the presented multicomponent solids of **2** and **ap**, in which the molecules of both constituents, present as metastable tautomers (keto and pyridine-protonated, respectively), stabilize each other through a very strong hydrogen-bonding pattern.

Results and Discussion

Syntheses and the occurrence of polymorphic phases

Form **2-I** was synthesized from methanol, **2-II** from ethanol, and **2-III** from isopropanol. However, in some cases repeated reactions gave different products, in rare cases (≈10%) product **2-III** was obtained from ethanol, and in several cases a mixture of **2-I** and **2-III** was yielded from isopropanol. When the synthesis was conducted in *n*-propanol, an amorphous form of **2** was collected.

Even a slight excess of **ap** in the synthesis yielded a mixture of products **2-I** and **2·ap-I** (from methanol). When the aldehyde/amine ratio was 1:2, the product was exclusively dark-red **2·ap-I**. The same product was obtained when previously prepared **2** in either form (**2-I**, **2-II**, or **2-III**) was reacted with amine (molar ratio 1:1) in alcohols. When the same reaction was conducted in chloroform or acetonitrile, prolonged heating at reflux was needed to partially dissolve the amine. After filtration and the removal of remaining amine, thin pale orange needles of multicomponent **2·ap-II** were obtained, albeit in low yield (maximum yield 20%).

Solid-state studies

Structural studies

Crystal structures of forms **2-I**–**III** have been determined by diffraction on single crystals. In all three forms the molecules are present as keto–amino tautomers, as evidenced both by the electron difference maps (Figure 1) and by the bond lengths between relevant non-hydrogen atoms,[19] with the hydrogen

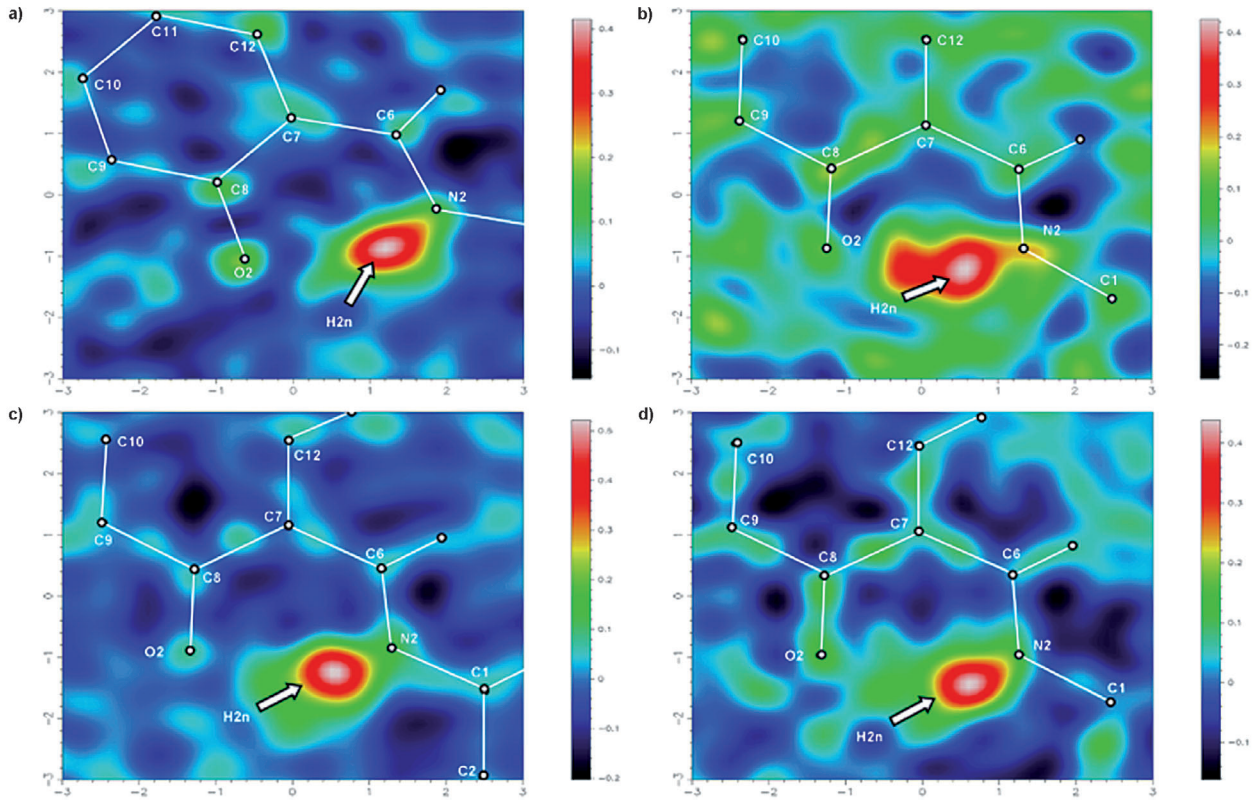

Figure 1. Electron difference maps showing the location of the hydrogen atom employed in the intermolecular hydrogen bond (H2n). a) Form **2-I**; b) form **2-II**, c) form **2-III**, d) bimolecular complex **2·ap-I**.

atom positioned on the N2 atom, while participating in the intramolecular hydrogen bond with the O2 atom (Figure 2, S1). The Schiff base molecule is of almost identical, approximately planar, conformation in all three forms, affording the smallest dihedral angle between the two aromatic rings in form **2-III** (2.2°) and a somewhat larger angle in **2-II** (7.6°) and **2-I** (8.9°).

Having in mind the molecular structure of **2**, it could be expected that the intermolecular O–H···N(py) hydrogen bond would represent the most robust intermolecular synthon,[25] even in the presence of the competing O–H···O(keto) one. However, the predominant intermolecular interaction in all

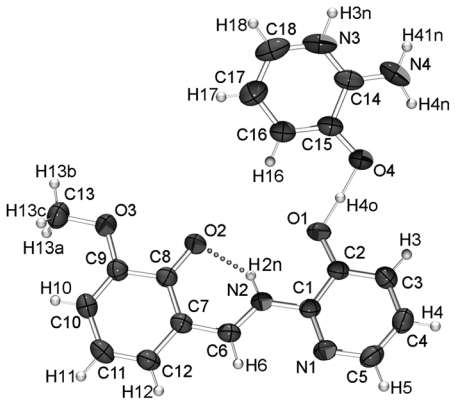

Figure 2. Molecular structure of the complex of **2** and **ap** (from crystal structure of the form **2·ap-I**) with the atom labeling scheme. The same labeling scheme is used for the Schiff base molecule **2** in forms **2-I–III**.

three polymorphs is the O1–H1o···O2 hydrogen bond and the pyridine nitrogen is not involved in any significant intermolecular contact. The dominant supramolecular synthon in the crystal structure of form **2-I** is hydrogen-bonded centrosymmetric dimer ($R_2^2(18)$, Figure 3a). As hydroxyl groups of both

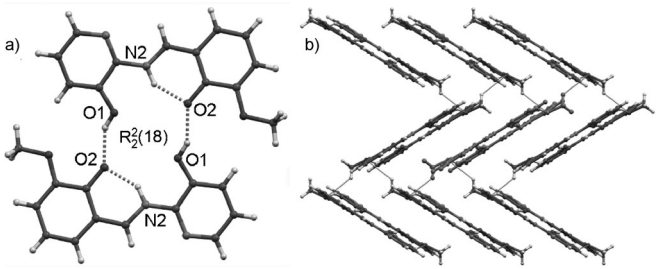

Figure 3. Crystal structure of form **2-I**. a) Hydrogen-bonded centrosymmetric dimers (O1–H1o···O2; 2.586 Å, 150.0°); b) packing of dimers into layers through weak hydrogen bonds (C13–H13b···O3 of 3.313 Å).

molecules participate in the formation of dimers, there are no strong hydrogen-bond donors remaining for further interconnection of molecules into the crystal. Therefore, the dimers pack into the crystal with only very weak C–H···O hydrogen bonds between methoxy groups of neighboring dimers interconnecting the molecules into layers (Figure 3b).

Unlike in the structure of form **2-I**, in the structures of forms **2-II** and **2-III** each molecule acts as a hydrogen donor to one neighbor and an acceptor to another, which leads to formation

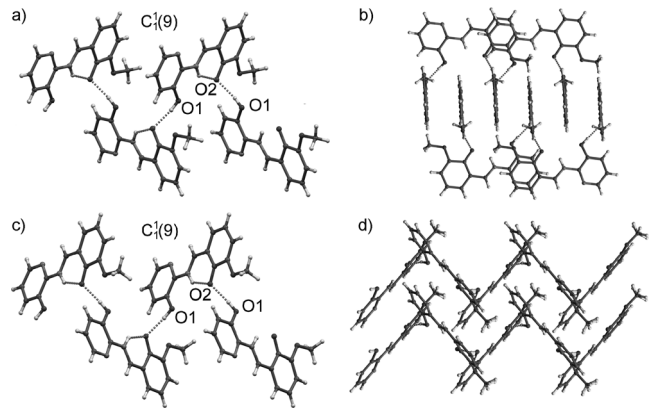

Figure 4. Crystal structures of forms **2-II** and **2-III**. a) Hydrogen-bonded chains in the structure of **2-II**; b) packing of neighboring chains in the structure of **2-II**; c) hydrogen-bonded chains in the structure of **2-III**; d) packing of neighboring chains in the structure of **2-III**.

of hydrogen-bonded $C_1^1(9)$ chains (Figure 4a and c). The chains in both structures are very similar; the O1–H1o···O2 hydrogen-bond lengths and angles have very close values in both structures (2.636 Å, 168.7° in **2-II**; 2.659 Å, 165.7° in **2-III**), and in both cases the chains form helices about screw twofold axes with almost identical dihedral angles between the mean planes of neighboring molecules (84° in **2-II** and 81° in **2-III**). In spite of these similarities, the overall crystal structures of the two polymorphs are quite dissimilar, due to large differences in further packing of the chains to form the crystal. In form **2-II** the chains are interconnected by two long C–H···O hydrogen bonds; C6–H6···O1 of 3.472 Å and C12–H12···O1 of 3.406 Å into layers perpendicular to the crystallographic *a* axis. The C–H···O bonds occur between the approximately perpendicular molecules (dihedral angle of 84°), and lead to stacking of (planar) Schiff base molecules along the crystallographic *b* axis (Figure 4b and d).

In the form **2-III** the chains are interconnected through C12–H12···N1 interactions of 3.459 Å, so that each molecule is a C–H donor to a molecule from one neighboring chain and an acceptor to a molecule of another, which leads to a 3D structure of chains interconnected by C–H···N contacts. The differences in packing modes of the two forms lead to a difference in their densities—stacking in the structure of **2-II** being a very efficient packing mode leads to its approximately 2.5% higher density (1.423 g cm^{-3}) relative to **2-III** (1.387 g cm^{-3}).

When an excess of **ap** was used in the synthesis of the Schiff base, the latter compound cocrystallized with unreacted **ap** forming what looked at first glance to be a 1:1 molecular salt (**2·ap-I**). The conformation of the Schiff base molecule is mostly unchanged from those in the three polymorphs, although the hydroxyl group of the **ap** ring has apparently been deprotonated. The heterocyclic nitrogen atom of the **ap** molecule is protonated and participates in a hydrogen bond with the oxygen of the keto–imino group of the neighboring Schiff base molecule (N3–H3n···O2 of 2.669 Å). The same Schiff base molecule is also the acceptor of the hydrogen bond with the *o*-amino group (N4–H4n···O1 of 2.879 Å). However, the most interesting feature of the supramolecular assembly is an extremely short hydrogen bond between the hydroxyl group of the **ap** and a hydroxyl group of another neighboring Schiff base molecule (O4–H4o···O1 of 2.454 Å). This hydrogen bond is almost linear (OHO angle of 176°), with similar O–H distances (O4–H4o of 1.193 Å and H4o···O1 of 1.262 Å), which places the hydrogen atom only 0.03 Å from the midpoint between the two oxygen atoms, thus rendering the hydrogen bond almost symmetrical. Furthermore, a closer inspection of the electron density map reveals that, although the position of the hydrogen atom corresponds to the maximum of the electron density, the electron density is in fact smeared between the O4 and O1 oxygen atoms along the direction of the hydrogen bond (Figure 5b). Because of this it is impossible to unambiguously maintain that the hydrogen atom is bonded to O4 rather than O1. The description of **2·ap-I** as a "salt" comprising a protonated **ap** and deprotonated **2** is therefore unsatisfactory, and the structure is equally well describable as a cocrystal of neutral **2** with zwitterionic **ap**.

Inclusion of the **ap** into the structure has no effect on the tautomerism, and the molecule of **2** in complex **2·ap-I** is also present as a metastable keto tautomer. This again can be brought into connection with the hydrogen bonding, since the O2 atom is here also an acceptor of a strong hydrogen bond (N3–H3n···O2). In fact, the hydrogen-bonding motif structure

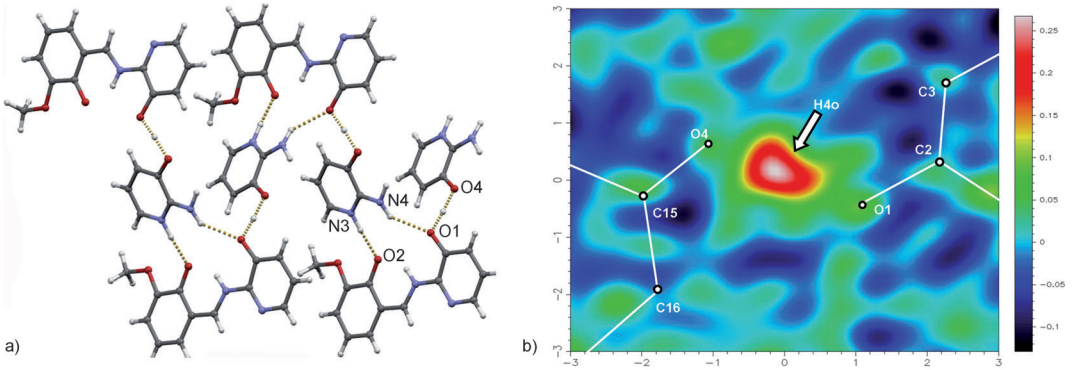

Figure 5. a) Crystal packing of the **2·ap** bimolecular complex **2·ap-I**. b) Electron density map showing the position of the hydrogen atom within the O4···H4o···O1 hydrogen bond.

of **2·ap-I** very much resembles the chains in the structures of forms **2-II** and **2-III**, with **ap** molecules interposed as bridges between molecules of **2** (Figure 5a). The hydrogen-bonding network can therefore be said to stabilize the structure comprising two molecules, each of which is present as a higher-energy tautomer.

Solid-state CP-MAS NMR and IR spectroscopy

^{13}C and ^{15}N solid-state NMR (SSNMR) experiments provided important information about Schiff base **2**, the protonation state of **ap** in **2·ap-I**, and the structurally unsolved polymorph of **2·ap** complex, **2·ap-II**. The results, in combination with the spectroscopic and/or X-ray diffraction structural studies, clearly demonstrated the presence of Schiff base in the keto form. For better assignment of spectra, we also applied the ^{1}H–^{13}C Lee–Goldburg cross-polarization magic angle spinning (CP-MAS) NMR technique (Figure S3 in the Supporting Information). ^{13}C signals of the imine carbon (C6) and carbon C8 located at $\delta \approx 140$ and 169 ppm, respectively, along with the ^{15}N signal for the imine nitrogen (N1) present at $\delta \approx -220$ ppm (Figure 6) (Figure 6). Apart from them, signals of C2 on the pyridine ring of the Schiff base molecule are of interest as this atom bears the OH group involved in the hydrogen bonding. These signals appear at $\delta \approx 144$ and 145 ppm in the ^{13}C CP-MAS spectra of **ap** and Schiff base, respectively, whereas in polymorphs **2·ap-I** and **2·ap-II** the signals of C2 and C15 are only tentatively assigned in the range $\delta \approx 146$–152 ppm (Figure 6). The details of the hydrogen-bonding pattern for **2·ap-II** is further given by ^{1}H MAS spectra, in particular the very strong hydrogen bond observed in form **2·ap-I** has given rise to a ^{1}H signal at $\delta \approx 17.9$ ppm. The occurrence of a similar peak ($\delta \approx 18.18$ ppm) also in form **2·ap-II** is strong evidence of the presence of the same hydrogen-bonding arrangement (O4···H4o···O1; see Figure S4 in the Supporting Information).

The differences in hydrogen bonding between the two multicomponent solids **2·ap-I** and **2·ap-II** can be clearly seen in their vibrational spectra. In the range of 3300–2500 cm^{-1}, two medium-strong bands correspond to N–H stretching vibrations of the amino group. In **2·ap-I**, the band at 3316 cm^{-1} is broad and weaker than that at 3448 cm^{-1}, thus suggesting involvement of one N–H group in strong intermolecular hydrogen bonding, as confirmed by the X-ray structural studies. In **2·ap-II**, both bands (3465 and 3355 cm^{-1}) are sharp, which indicates that the respective amino group is not involved in strong hydrogen bonding. The medium-strong band at 1650 cm^{-1} (**2·ap-I**) or 1663 cm^{-1} (**2·ap-II**) confirms the protonation of the pyridine nitrogen atom,[25a,26] and the strong band at 1619 cm^{-1} for both forms confirms that the Schiff bases are still in the keto form.[9,11]

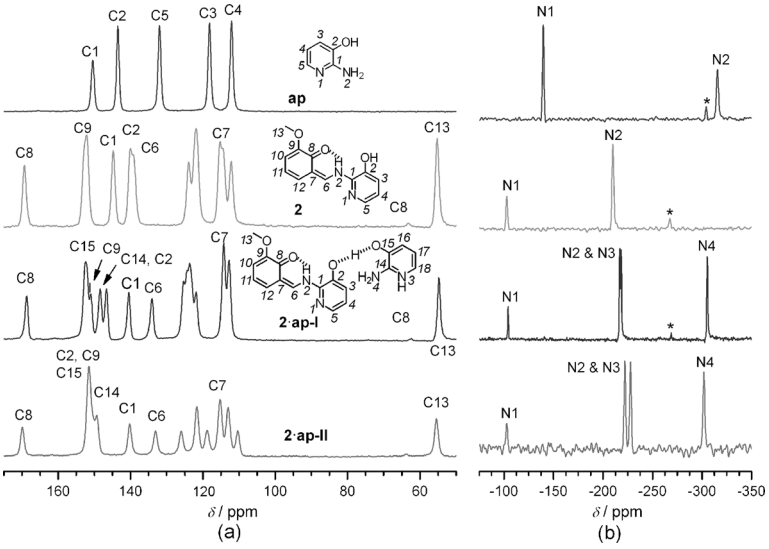

Figure 6. a) ^{13}C CP-MAS and b) ^{15}N CP-MAS NMR spectra of **ap**, Schiff base **2**, and polymorphic forms **2·ap-I** and **2·ap-II** of complexes (Table S7 in the Supporting Information). Asterisks (*) denote side bands.

confirmed that carbon C6 bears the keto functionality involved in strong intramolecular hydrogen bonding with the amino nitrogen N2. In imino Schiff bases, the ^{13}C signal for enol carbon (C8) and the carbon C6 connected to imine nitrogen would be located at $\delta \approx 160$ and 166 ppm, respectively,[11] whereas the imine nitrogen is in the literature assigned at $\delta \approx -100$ ppm.[9b] The signal at $\delta = -103$ ppm in the ^{15}N CP-MAS spectra of **2**, **2·ap-I**, and **2·ap-II** is assigned to pyridine nitrogen N1. In both **2·ap-I** and **2·ap-II** the **ap** nitrogen N3 is protonated (^{15}N signal $\delta \approx -220$ ppm) and the ^{15}N signal of primary amine group NH_2 is at $\delta \approx -303$ ppm. Although the ^{15}N SSNMR spectra of polymorphs **2·ap-I** and **2·ap-II** are similar, significantly different ^{13}C CP-MAS spectra support two different solid-state structures

Solution studies

Tautomeric equilibria and the potential of proton transfer in solution have been thoroughly investigated by NMR and UV/Vis spectroscopy, calorimetry, and potentiometry.

NMR spectroscopy

In the ^{1}H NMR spectrum of **2** in chloroform and acetonitrile, a broad signal corresponding most likely to a proton from O1 is observed at approximately $\delta \approx 12.7$ and 13.3 ppm, respectively, whereas the signal of the other hydroxyl proton could not be detected.[27] For that reason, these signals could not be used to gain insight into the position of the tautomeric equilibrium in solution. The dependence of the position of the azomethine proton signal (upfield shift in methanol with respect to aprotic solvents) indicated that the keto tautomer is more

abundant in methanol than in other solvents.[11] However, the resonance of the azomethine proton for the keto tautomer is expected at significantly lower chemical shifts, thus suggesting that although the keto tautomer is present in a significant amount, the enol–imino form is predominant even in methanol.[28] In the COSY spectrum of **2**, interaction between protons resonating at $\delta \approx 14.03$ ppm ascribed to O2···H···N2 and the azomethine proton at $\delta \approx 9.43$ ppm was detected (Figure S12 in the Supporting Information). The existence of this cross-peak proves the presence of the keto tautomer in DMSO solution, since the interaction between H1o and the azomethine proton would not be expected in the enol form. The intensity of this cross-peak is, however, very weak due to the low abundance of the keto form. The same interaction was noticed also in the NOESY spectrum of **2**.

The ^{1}H NMR spectrum of **2·ap-I** in DMSO is roughly a combination of the individual spectra of **2** and **ap** with no protonated pyridine observed in solution (Figure S14 in the Supporting Information). The assignment of the signals is given in Table S4 in the Supporting Information. However, the signals corresponding to resonance of hydroxyl and amino protons of **ap** are both shifted upfield with respect to free **ap**, thus indicating that interaction between **2** and **ap** molecules is established in solution. To ascertain this finding, the ^{1}H NMR spectrum of **2** with an excess of **ap** added to the solution was recorded. The signal assigned to the proton connected to O1 of **2** could not be found in this spectrum. Tentatively, this could be explained by the formation of a strong hydrogen bond with **ap**.

An analogous experiment was carried out in acetonitrile, in which formation of the **2·ap** complex was again suggested by the disappearance of the H1o signal of **2** upon addition of an excess of **ap** (Figure S16 in the Supporting Information). However, no changes in the positions of signals corresponding to protons on the pyridine part of the molecule were observed. Notably, the broad singlet in the spectrum of **2·ap-I** recorded in chloroform, corresponding to the O1H proton, was positioned at a slightly lower chemical shift in the spectrum of **2·ap-I** than in that for **2**. Although this implies that interaction between **ap** and **2** is established in chloroform, the observation alone could not be considered as a proof of the complex formation in this solvent, since it is difficult to determine the exact position of the broad signal.

The ^{1}H NMR spectra of **2** and **2·ap-I** in [D$_3$]MeCN were recorded at -25 and 25 °C (Figure S17 in the Supporting Information). The only significant change caused by lowering the temperature was a downfield shift of the O2···H···N2 proton signal accompanied by its sharpening. That could be explained by taking into account the presence of the aforementioned strong intramolecular hydrogen bond in **2**.

UV/Vis spectroscopy

In the UV/Vis spectrum of compound **2**, two well-defined peaks at approximately 280 and 350 nm appeared in all solvents. As was the case with Schiff base **1**, an additional band at higher wavelengths (centered at 471 nm) occurred in methanol, accompanied by a decrease in absorbance at 350 nm with respect to other solvents. This additional band can be ascribed to the absorption of the keto tautomer.[29] Also, the increase in intensity of the high-wavelength band was more pronounced in the case of **2** as compared to **1**. However, even though the signal corresponding to the keto form was observed in all solvents, the enol tautomer was still predominant in all cases.

As in the case of the NMR results, the UV/Vis spectra of forms **2·ap-I** and **2·ap-II** closely match the linear combination of individual spectra of **2** and **ap**. The formation of **2·ap** complex was not detected by UV/Vis spectroscopy (Figures S24–S27 in the Supporting Information) in any of the tested solvents (MeOH, $CHCl_3$, MeCN, DMSO), that is, no significant spectral changes occurred during titration of **2** with **ap**. This is most likely caused by overlapping of absorption bands of **ap** and **2**, as well as by the low concentrations of both **ap** and **2**, which could cause a low extent of the complexation reaction. Furthermore, the formation of the hydrogen-bonded complex might not have a pronounced impact on the spectral properties of **2**, and therefore could not be detected by UV/Vis spectroscopy.

Calorimetry

By employing calorimetry as a tool for studying the interactions between **2** and **ap**, we were able to overcome the limitations encountered using UV/Vis spectroscopy. Exothermic signals were observed upon addition of **ap** to a solution of **2** in DMSO, which indicated the formation of a complex. Relatively high concentrations of the reactants were used in the microcalorimetric titrations, so the extent of complexation reaction was high enough to enable estimation of the stability constant of the complex formed, in spite of relatively low values of both formation constant and the corresponding reaction enthalpy. The assessed values amount to $K = 69\ \mathrm{mol^{-1}\,dm^3}$ and $\Delta_r H = -0.88\ \mathrm{kJ\,mol^{-1}}$. The rather low $\Delta_r H$ value can be explained by taking into account the hydrogen-bond acceptor property of DMSO. Namely, during the complexation, a number of hydrogen bonds between the reactants and the solvent molecules must be disrupted to allow formation of hydrogen bonds between **2** and **ap**. The outcome of these two energetically opposite processes can be an almost isoenthalpic reaction. A relatively high and favorable reaction entropy ($\Delta_r S \approx 33\ \mathrm{J\,K^{-1}\,mol^{-1}}$), calculated from the calorimetric data, is in accordance with this consideration. Unfortunately, based on the experimental data it was not possible to resolve whether intramolecular proton transfer in **ap**, that is, formation of a zwitterion, was induced by complex formation, as observed in the solid state.

Protonation equilibria

To gain further insight into the influence of the methoxy group on the properties of the studied Schiff bases, as well as into the nature of the complex between **2** and **ap**, protonation equilibria of **1**, **2**, and **ap** in methanol were studied by potentiometric–spectrophotometric titrations (Figures S28–S33, re-

spectively, in the Supporting Information). Several acid–base equilibria are associated with the Schiff bases investigated in this work: dissociation of the hydroxyl groups of salicylaldehyde and pyridine subunits as well as the protonation of the nitrogen atom in the aminopyridine ring (Scheme 1). However, only the equilibria at pH > 9, that is, (de)protonation of OH groups, could be investigated due to the hydrolysis of the compounds in acidic medium. The determined protonation constants are given in Table 1, and the electronic absorption

Table 1. Protonation constants of compounds **1**, **2**, and **ap** in methanol at $T = (25.0 \pm 0.1)^{\circ}C$, $I_c = 0.01$ mol dm^{-3} (Et_4NClO_4) determined by simultaneous potentiometric–spectrophotometric titrations.

Compound	log K [mol^{-1} dm^3] ± standard deviation		
	NH + (py)	OH(sal)	OH(py)
1	–	11.68 ± 0.02 (11.48 ± 0.01)[a]	12.28 ± 0.02
2	–	11.59 ± 0.01 (11.39 ± 0.01)[a]	12.58 ± 0.02
ap	8.31 ± 0.01 (8.29)[a]	–	12.67 ± 0.01

[a] Determined by potentiometric titration. py = pyridine, sal = salicylaldehyde.

spectra of different protonation forms, as well as distribution diagrams for the investigated compounds, are presented in the Supporting Information. The equilibrium constants corresponding to protonation of the OH group on the salicylaldehyde subunit for both **1** and **2** were additionally determined by potentiometric titrations. The values obtained by this method were in good agreement with those determined by simultaneous pH–spectrophotometric measurements (Figures S38–S41 in the Supporting Information).

As expected, the protonation constants of **1** and **2** are similar (Table 1). The difference in protonation constant of the O2–H group can be readily explained by an inductive effect of the methoxy group in the *ortho* position. It should be pointed out that the assignment of the determined equilibrium constants is not straightforward. Namely, both OH groups are expected to exhibit similar protonation properties and it is difficult to establish whether the hydroxyl group from salicylaldehyde or pyridine subunits of **2** is more prone to dissociation. The assignment was made based on much more pronounced spectral changes induced by the first ionization process. Namely, the transition causing the absorption at 352 nm involves the excitation of the π-electronic system of the whole molecule.[30] The O2–H group is involved in the intramolecular resonance-assisted hydrogen bonding, so the dissociation of this group should cause more pronounced spectral changes. In addition, the ionization constant of **ap**, which is unambiguously assigned to the deprotonation of the O4–H group, is similar to the second protonation constant of **1** and **2**. This implies that these equilibrium constants are associated with the same type of functional group. Notably, the protonation constants of both hydroxyl groups of the Schiff base are more than 1000 times greater than that determined for the NH group of **ap**. Hence, the proton transfer from OH groups to the pyridine nitrogen atom does not take place in solution, and the ionic form detected in the solid state can only be formed by supramolecularly induced intramolecular proton transfer as the complex is formed and is evidently stabilized by crystal forces.

Computational studies

Tautomeric formulation of the lead compound detected in solution and in the solid state is a consequence of the intra- and intermolecular interactions that can induce a shift in the tautomeric equilibrium. DFT calculations were used to rationalize the experimental findings.

Tautomerism

A detailed conformational search was conducted to identify isomers of compound **2**. The representative isomers are depicted in Figure 7a and Figure S42 in the Supporting Information. All reported energies are given with respect to the most stable

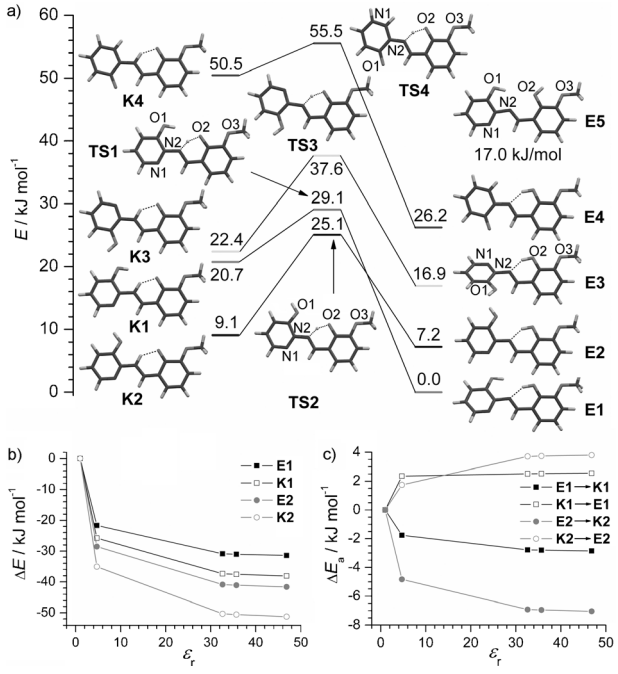

Figure 7. a) Energies of the isomers of **2** relative to the most stable enol–imino form **E1** in MeOH. b) Stabilization energies relative to the gas phase of **K1**, **K2**, **E1**, and **E2** in solvents of different permittivity ($CHCl_3$, $\varepsilon_r = 4.71$; MeOH, $\varepsilon_r = 32.61$; MeCN, $\varepsilon_r = 35.69$; DMSO, $\varepsilon_r = 46.83$) that are implicitly introduced. c) Keto–enol energy barriers for **K1**/**E1** and **K2**/**E2** in various solvents relative to the analogous energy barrier in the gas phase. TS = transition state.

isomer **E1**. Implicit solvent modeling lowers the relative energies of all forms (Table S8 in the Supporting Information). Individual enol–imino forms (**E1**–**E4**) are more stable than their tautomers, the keto–amino forms (**K1**–**K4**), as observed by spectroscopic experiments. The energy decrease is significant when $CHCl_3$ (relative permittivity $\varepsilon_r = 4.71$) and especially MeOH ($\varepsilon_r = 32.61$) are implicitly introduced. Modeling of MeCN

($\varepsilon_r = 35.69$) and DMSO ($\varepsilon_r = 46.83$) causes only a small further stabilization of all species compared to the energies in MeOH (Figure 7b and Table S8 in the Supporting Information). The important finding is that the keto–amino forms are more stabilized than their tautomers in the same environment (Figure 7c). The energy barriers for the enol-to-keto tautomerization for the two lowest-lying tautomeric pairs, that is, **K1**/**E1** and **K2**/**E2**, decrease with the increase of solvent polarity, whereas the opposite is calculated for the keto-to-enol energy barriers (Figure 7c). Structures **K3** and **E3**, analogous to those observed in our previous work,[6] are positioned more than 16.5 kJ mol^{-1} above the most stable form even in DMSO (Figure S42 and Table S14 in the Supporting Information). The most stable zwitterionic pair **K4**/**E4** is very high in energy, and again the enol–imino tautomer is preferred (Figure 7a and Figure S42 in the Supporting Information).

Explicit solvent–solute interactions influence the relative stabilities of the described solute species. We decided to test whether the stabilization of O1H, O2/O3Me, or pyridine nitrogen N1 groups through hydrogen-bonding interactions with solvent molecules could cause a significant decrease in energy differences between the keto and enol isomers. Only the two most stable tautomeric pairs, **K1**/**E1** and **K2**/**E2**, were tested. One explicit solvent molecule ($CHCl_3$, MeOH, MeCN, or DMSO) was placed at several positions around the investigated molecule and the energies of these keto and enol solvent–solute pairs were compared to each other and to the individual solvent and solute molecules. Tables S9–S18 in the Supporting Information collect the chosen optimized geometries and their energies for all four solvents.

The most important finding is that the introduction of one hydrogen-bonding interaction of MeOH, MeCN, or DMSO with the O1H group causes the largest stabilization of both keto and enol forms (26.3–57.7 kJ mol^{-1}) if compared to the interactions of these solvents with the pyridine nitrogen N1 or the O2/O3Me (Tables S9–S17 in the Supporting Information). Furthermore, in solvent–solute pairing through the O1H group in MeOH or DMSO, the energies of the keto form **K1** and its accompanying transition-state structure **TS1** are especially reduced (see Figure 8). Differences in the stabilization of the keto form with respect to the enol form are 7.9, 13.9, and 20.2 in MeCN, DMSO, and MeOH, respectively. Keto tautomer **K1** becomes almost equal in energy to its enol pair **E1**, whereas the stabilization of the transition state **TS1** makes the activation barrier for the pair **K1**/**E1** lower and more symmetric than in the case of the isolated solute molecule.

Computed results indicate that stabilization of the O1H group, which is better accomplished in more polar and/or hydrogen-bonding prone solvents (MeOH, MeCN, or DMSO), leads to the overall reduction of the energy difference between the keto and the enol tautomers. If the described change in stability of tautomers is induced, the equilibrium would shift toward the keto form and probably generate a sufficient amount of the keto form in solution for its detection by spectroscopic methods. Interestingly, differences in the stabilization of **K2** and **E2** with one solvent molecule are small (maximum 2.6 kJ mol^{-1} in DMSO) and cannot cause or explain the observed shift in the tautomeric equilibrium (Figure S44 in the Supporting Information).

The interaction of the solvent molecule (MeOH, MeCN, or $CHCl_3$) with O2/O3Me stabilizes **K1** and **K2** more than **E1** and **E2** (Tables S11–S17 in the Supporting Information). Interactions of other functional groups with the solvent molecules do not significantly change the overall energy relations between the tautomers (Tables S9–S17 in the Supporting Information). We could not locate a tautomeric pair in $CHCl_3$ with the keto form more stable than the enol form for **K1**/**E1** or **K2**/**E2** pairs, which confirms the experimental domination of the enol form in less polar and non-hydrogen-bonding donor solvents (Tables S16 and S17 in the Supporting Information).

Dimeric structures

Until now we have focused on the monomeric forms, which most likely dominate in diluted solutions and highly polar solvents. However, X-ray experiments reveal that the O–H···O hydrogen bonding ($R_2^2(18)$) leads to the formation of dimers (or chains). In this respect, we have modeled various types of possible dimeric structures to examine their relative stabilities and tautomerization. The calculations show that the keto–amino dimers $(\mathbf{K2})_2$ are the most stable species in the gas phase and in MeOH, followed by the "mixed" dimer (**K2**)(**E2**) at about 16 kJ mol^{-1} and the enol–imino dimer $(\mathbf{E2})_2$ at about 29 kJ mol^{-1} with respect to $(\mathbf{K2})_2$ (see Figure 9).

All analogous dimers exhibit only small energy differences (< 1.7 kJ mol^{-1}) on comparing the gas phase and MeOH. Thus, in solution when the concentration of the compound is sufficiently high, the keto–amino dimers may form leading to the isolation of keto–amino crystal forms.

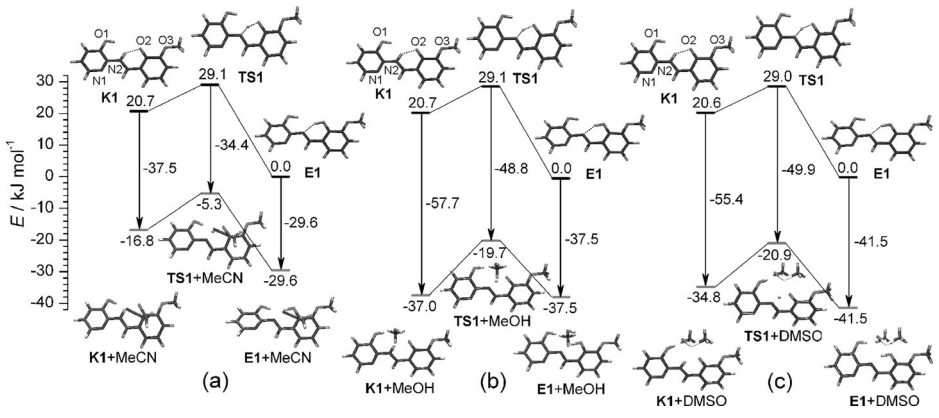

Figure 8. Energies of **E1**, **TS1**, and **K1** without (top) and with (bottom) one solvent molecule close to the O1H group relative to the individual **E1** and the solvent molecules; a) MeCN, b) MeOH, and c) DMSO.

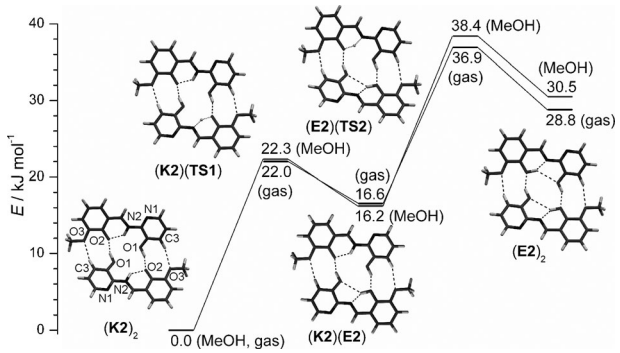

Figure 9. Energies of the possible dimer forms of **2** relative to the diamino dimer calculated in the gas phase and using IEF-PCM MeOH (IEF-PCM = polarizable continuum model using the integral equation formalism).

Complexes of Schiff base 2 and ap

Compounds **2·ap-I** and **2·ap-II** crystallize in the reaction of **2** with an excess of **ap**. In the structure of **2·ap-II**, the **ap** interacts with **2** in two ways: through discrete O1···H···O4 and $R_2^2(13)$ hydrogen-bonding interactions (Figure 10). Calculations were used to identify the most stable tautomeric form for the two experimentally observed structural motifs. As the crystallization and spectroscopic measurements were conducted in $CHCl_3$, MeOH, and DMSO, these solvents were used in calculations. In general, the keto forms analogous to the experimental motifs (from MeOH) were identified as the most stable structures in polar solvents, MeOH and DMSO (Figure 10).

The $R_2^2(13)$ structural motif was modeled in two ways testing the influence of the H position on the stability of the isomers (Figure 10a). Keto structures with the cationic **ap** and deprotonated O1 in anionic Schiff base **2** (**KZ1-1**) are lower in energy if compared to structures with neutral Schiff base and zwitterionic **ap** (**KZ1-2**). If only orientations depicted in Figure 10a are considered, the substantial energy differences between **KZ1-1** (or **KZ1-2**) and their possible isomers imply that the keto structure with the protonated pyridine nitrogen analogous to the experimental motif is highly preferred.

In the case of the O1···H···O4 interaction of two molecules, two orientations were detected (Figure 10b). The open structures with a tilted **ap** molecule with respect to the Schiff base occur in all solvents, whereas the closed structures with additional C16–H16···O2 interaction (**KN2-2** and **EN2-2**) are detected only in the gas phase and in the low-polarity solvent $CHCl_3$. Neutral keto form **KN2-1** is the most stable in MeOH and DMSO. Small energy differences between the neutral tautomers **KN2-1** and **EN2-1** ($< 3\ kJ\,mol^{-1}$) indicate that the hydrogen-bonding interaction with the O1H group is again a significant factor for the stabilization of the Schiff base in the keto form. This result agrees well with the previously described study of the solvent interaction with the O1H group.

Relative stabilities of polymorphic phases

To relate the computational results and experiment, various solid-state and solvent-mediated techniques were employed to establish the relative stabilities and interconversion conditions

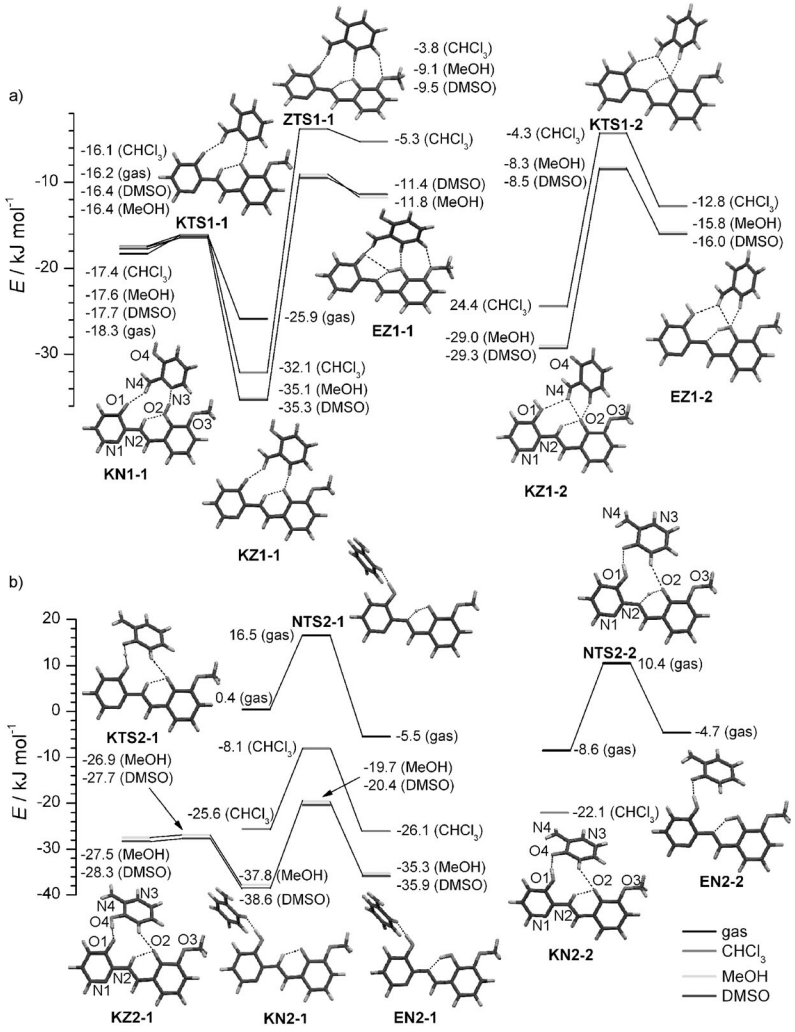

Figure 10. Possible complexes of **2** with **ap** corresponding to two experimental structural motifs: a) $R_2^2(13)$ and b) discrete O–H···O hydrogen bonding. Energies are given with respect to the sum of energies of the most stable individual imine form **E1** and the most stable pyridine form **P1**.

among polymorphic forms and also to test their possible photochromic or thermochromic properties.

Thermal measurements

Forms **2-I**, **2-II**, and **2-III** were heated to 400 °C in nitrogen atmosphere to establish the conditions for their possible interconversion. All three compounds display weak endothermic events before a strong endotherm (melting). Melting is followed by immediate decomposition of the sample (strong exotherm). Analyses (powder X-ray diffraction (PXRD), IR spectroscopy) showed that **2-I** is stable below the melting point (176 °C) whereas form **2-II** transformed to an amorphous product by heating to 150 °C. Form **2-III** displayed a weak and broad endotherm in the range of 120–140 °C and a broad endotherm ascribed to melting, followed by two consequent exotherms. PXRD analysis revealed that in the range of 120–140 °C form **2-III** partially transformed to form **2-I**. We repeated the heating experiment and kept the sample at 150 °C for an hour, but the final product was again a mixture of forms **2-I** and **2-III**. Therefore, the broad endotherm (melting) and the two exotherms can be tentatively ascribed to melting and decomposition of forms **2-I** and **2-III**. The melting point of **2·ap-I** is 174 °C, whereas that of **2·ap-II** is 163 °C. Compounds **2·ap-I** and **2·ap-II** do not experience any phase transition below the melting point (PXRD), and they both decompose immediately after melting, which is again evidenced by a strong exotherm.

Competitive slurry experiments

Slurry experiments[31] were performed to establish the relative stabilities of the three polymorphs of **2** and the multicomponent forms **2·ap-I** and **2·ap-II**. All slurry experiments were conducted at room temperature. Ternary mixtures of forms **2-I**, **2-II**, and **2-III** (in *i*PrOH or EtOH) were stirred on a magnetic stirrer and samples were taken out from the cell after 24, 43, and 170 h and analyzed by PXRD and FTIR spectroscopy. After the last sampling, a small volume of MeOH was added to the reaction mixture and the stirring was continued for an additional 24 h. Analyses revealed that polymorphic forms **2-I**, **2-II**, and **2-III** are present in almost unchanged relative ratios after 170 h of stirring in *i*PrOH. However, small changes in the diffractograms suggested that form **2-I** diminished slightly, which was more evident after addition of methanol to the slurry mixture. After an additional 24 h of stirring the reaction slurry in a mixture of *i*PrOH/MeOH (5:1 volume ratio), form **2-I** completely disappeared and form **2-III** was the dominant component in the product, together with traces of form **2-II**. However, prolonged stirring of this mixture (additional 48 h) resulted again in a mixture of forms **2-II** and **2-III**, so no pure product was obtained in the slurry experiments. Similar results were obtained when binary mixtures of forms **2-I**, **2-II**, and **2-III** were stirred in EtOH.

Forms **2·ap-I** and **2·ap-II** were stirred in acetonitrile for 6 days and again no complete transformation to either of the tested forms was observed. However, slurry experiments in this particular case proved to be sensitive to the solvent used. Addition of a small volume of methanol (20% volume fraction) resulted in complete transformation of form **2·ap-II** to form **2·ap-I**.

Mechanochemical interconversions

Forms **2-I**–**III** are stable upon grinding and no phase transition was observed after 30 min of neat (or dry) grinding (NG) or liquid-assisted grinding (LAG) with MeOH, EtOH, or *i*PrOH as liquid additives (ball mill operating at 25 Hz, one ball weighing 1.33 g, 15 μL of liquid for 150 mg of reaction mixture). Forms **2·ap-I** and **2·ap-II** were highly sensitive to the liquid used for LAG. In NG, no transformation between forms **2·ap-I** and **2·ap-II** was observed, but LAG with acetonitrile or chloroform converted **2·ap-I** to **2·ap-II** (30 min, 25 Hz) quantitatively. On the other hand, **2·ap-II** was transformed to form **2·ap-I** by LAG with MeOH. It is evident that the use of mechanochemical procedures enabled fast and complete transformation of form **2·ap-I** to form **2·ap-II**, which was not possible in any solution or slurry experiment.

Conclusion

The results presented demonstrate the importance of directional supramolecular interactions to achieve the formation of metastable tautomers in solution and in the solid state. The investigated compound **2** is more stable as the enol form in the gaseous phase and in solution, but upon introducing a suitable hydrogen-bond donor, the hydrogen bonding results in the shift of the equilibrium towards the metastable keto tautomer. This is especially emphasized in the cocrystal **2·ap**, in which both components are stabilized as their metastable tautomers (protonated **ap** and **2** in keto form) through a rich supramolecular interaction pattern. This work also shows that supramolecular stabilization of metastable tautomers is not only applicable for multicomponent solids, but also for the monocomponent, as was the case here for three polymorphs of the keto tautomer of **2**. This stabilization has led to the occurrence of the less expected supramolecular synthon O–H···O(carbonyl) in the structures of all three forms of **2**, and not the robust O–H···N(py). We believe that upon comprehending the complex interplay between supramolecular interactions and emergence of specific tautomeric forms, one can establish the foundation for the synthesis and wider application of functional tautomeric solids.

Experimental Section

Detailed descriptions of the experimental procedures, IR spectra, and DSC curves of all the isolated solids can be found in the Supporting Information.

Mechanochemical routines

All forms were neat ground using a Retsch MM200 ball mill (25 Hz) for 30 min. Samples were ground in steel jars (5 mL inner volume) using one 7 mm (≈1.3 g) steel ball. After such treatment, PXRD patterns and IR spectra were collected for all samples. Mechano-

chemical reactions were recently reported as a highly efficient method for controllable synthesis of polymorphic Schiff base.[32] However, our attempts to synthesize **2-I**–**III** by mechanochemical routines were unsuccessful, resulting in an amorphous black mixture of products (NG). Even when hydrolysis was prevented by LAG (MeOH), the main product in the grinding jars was multicomponent **2·ap-I**, which could be due to the local excess of the amine during the milling process. When the polymorphs of ligand were reacted with the amine by using NG, **2·ap-I** was obtained (highly amorphous) in a mixture with starting compounds. Pure **2·ap-I** was obtained from binary mixtures of **2-I**, **2-II**, or **2-III** and **ap** (1:1) by LAG with methanol. LAG reaction of **2-I**--**III** with **ap**, by using chloroform or acetonitrile, yielded product **2·ap-II** quantitatively. In both cases, mechanochemical routines proved beneficial over solution approaches in terms of time, energy, and volume of solvent used for reaction.

Spectrophotometry

UV/Vis spectra were recorded using a double-beam Varian Cary 5 spectrophotometer equipped with a thermostatting device with temperature set at (25.0±0.1)°C. The optical path length used was 1 cm and the concentration of the compound was approximately 1×10^{-4} mol dm^{-3}. Spectrophotometric titrations of **2** with **ap** were carried out in methanol, acetonitrile, and a mixture of chloroform and 5% methanol (volume fraction) because of the low solubility of **ap** in chloroform. Titrant solution (**ap**) was added to the solution of **2** (2.5 mL, $c\approx1\times10^{-4}$ mol dm^{-3}) directly into the measuring cell. Concentrations of titrant solutions were 3.19×10^{-4} (MeOH), 4.92×10^{-4} (MeCN), and 1.42×10^{-4} mol dm^{-3} ($CHCl_3$/MeOH).

Potentiometry

The pH was measured using a combined glass electrode (Metrohm LL Micro glass electrode 6.0234.100) with the reference electrode compartment filled with a methanol solution (0.01 mol dm^{-3}) of Et_4NCl (Sigma–Aldrich, >99%,). The electromotivity of the cell was measured by a Metrohm 827 pH meter. Calibration of the cell was carried out by using three methanolic buffer solutions. The details of the calibration procedure are described elsewhere.[11] The solvent (methanol, HPLC grade, J. T. Baker) was kept under argon prior to preparation of solutions. All measurements were performed at (25.0±0.1)°C. Potentiometric data were processed by nonlinear regression analysis using the Hyperquad program.[33]

Spectrophotometric–potentiometric titrations

Methanol solutions of NaOH and HCl ($c\approx1\times10^{-3}$ mol dm^{-3}) were added to solutions of **ap** (8 mL, $c\approx1\times10^{-4}$ mol dm^{-3}) to set the pH at the desired value. In the case of Schiff bases **1** and **2**, only NaOH was added since hydrolysis of the compounds occurred in acidic solution. The spectra of the solutions at different pH values were recorded and the acquired data were processed by nonlinear regression analysis using the pHab program.[34] Ionic strength was kept constant at 0.01 mol dm^{-3} by adding Et_4NCl.

Potentiometric titrations

The protonation constants of the O2H group of **1** and **2** were additionally determined by potentiometric titrations, which were carried out by incremental addition of a standardized solution of NaOH ($c\approx5\times10^{-2}$ mol dm^{-3}) to a solution of **1** or **2** (8 mL, $c\approx3\times10^{-3}$ mol dm^{-3}) placed in a thermostatted vessel. Ionic strength was kept constant at 0.1 mol dm^{-3} by adding Et_4NCl. The protonation constant of pyridine nitrogen of **ap** was determined by potentiometric titration with $HClO_4$ ($I_c=0.1$ (Et_4NClO_4)).

Computational details

Calculations were carried out using Gaussian 09.[35] A density functional theory (DFT) approach with the ωB97X-D exchange-correlation functional was applied to better account for the intramolecular dispersion interactions.[36] A relatively large basis set, 6-311+G(2d,p), was used to minimize the intramolecular basis set superposition error.[37] For implicit solvation, a polarizable continuum model using the integral equation formalism (IEF-PCM)[38] was used to model the following solvents: chloroform ($CHCl_3$, $\varepsilon_r=4.71$), methanol (MeOH, 32.61), acetonitrile (MeCN, 35.69), and dimethyl sulfoxide (DMSO, 46.83). Frequency calculations identified all stationary points as minima (zero imaginary frequencies) or first-order saddle points (one imaginary frequency exhibiting atom displacements consistent with the anticipated reaction pathway). The nature of the transition structures was confirmed by intrinsic reaction coordinate (IRC) searches.

Solid-state NMR spectroscopy

^{13}C and ^{15}N cross-polarization magic angle spinning (CP-MAS) NMR spectra were obtained on an Agilent Technologies NMR System 600 MHz NMR spectrometer equipped with a 3.2 mm NB Double Resonance HX MAS Solids Probe. Larmor frequencies of carbon and nitrogen nuclei were 150.77 and 60.78 MHz, respectively. The ^{13}C and ^{15}N CP-MAS NMR spectra were externally referenced using hexamethylbenzene (HMB) and ammonium sulfate ($\delta\approx-355.7$ ppm with reference to nitromethane at $\delta\approx0.0$ ppm), respectively. Samples were spun at the magic angle with 16 kHz during ^{13}C measurement and with 10 kHz during ^{15}N measurement. For more precise assignment of ^{13}C spectra, we applied Lee–Goldburg CP-MAS NMR spectroscopy. ^{1}H–^{13}C Lee–Goldburg CP-MAS NMR measurements correlate only the nearest ^{1}H and ^{13}C nuclei and thus enable easier and more reliable assignment than the more common and robust (RAMP) CP-MAS measurements. In Lee–Goldburg CP-MAS measurements, ^{1}H magnetization is locked along the effective magnetic field, which is inclined at the magic angle with respect to the static magnetic field. In this way during the CP, block ^{1}H–^{1}H homonuclear dipolar interactions are efficiently suppressed. In our experiment a moderate proton radio-frequency power corresponding to a ^{1}H nutation frequency of 68 kHz was used for the Lee–Goldburg CP.

X-ray single-crystal diffraction experiments

Diffracted intensities were collected at room temperature by an Oxford Diffraction Xcalibur CCD diffractometer with graphite-monochromated $Mo_{K\alpha}$ radiation at 293 K using ω scans. Details of data collection and crystal structure refinement are presented in Table S1 in the Supporting Information. Programs CrysAlis CCD and CrysAlis RED[39] were employed for data collection, cell refinement, and data reduction. The structures were solved by direct methods. Refinement procedures by full-matrix least-squares methods based on F^2 values against all reflections included anisotropic displacement parameters for all non-H atoms. The positions of hydrogen atoms not involved in hydrogen bonding were positioned geometrically and refined by applying the riding model, whereas the hydrogen atoms involved in intra- and intermolecular hydrogen bonds were located from electron difference maps and refined isotropically. Calculations were performed with SHELXS97[40] and SHELXL97[41] (both operating within the WinGX[42] program pack-

age). Geometry calculations were done using PLATON[43] and PARST.[44] CCDC-1002814, 1002815, 1002816, and 1002817 contain the supplementary crystallographic data for this paper. These data can be obtained free of charge from The Cambridge Crystallographic Data Centre via www.ccdc.cam.ac.uk/data_request/cif.

Acknowledgements

The Ministry of Science, Education, and Sport of the Republic of Croatia is kindly acknowledged for financial support (Grant Nos. 098-0982915-2950, 119-1191342-1082, 119-1193079-3069, and 119-1191342-2960). Financial support of the Slovenian Research Agency (ARRS, P1-024) is acknowledged.

Keywords: keto–enol · metastable compounds · Schiff bases · supramolecular chemistry · tautomerism

[1] a) *Tautomerism: Methods and Theories*, (Ed.: L. Antonov), Wiley-VCH, Weinheim, **2014**; b) A. R. Katritzky, J. M. Lagowski, *In Advances in Heterocyclic Chemistry, Vol. 1*, (Ed.: A. R. Katritzky), Academic Press, New York, **1963**, pp. 311 – 338; c) J. Elguero, A. R. Katritzky, O. V. Denisko in *Advances in Heterocyclic Chemistry, Vol. 76*, (Ed.: A. R. Katritzky), Academic, San Diego, **2000**, pp. 2 – 64; d) J. Elguero, C. Marzin, A. R. Katritzky, P. Linda in *Advances in Heterocyclic Chemistry: Supplement 1*, Academic Press, New York, **1976**; e) B. Stanovnik, M. Tišler, A. R. Katritzky, O. V. Denisko in *Advances in Heterocyclic Chemistry Vol. 91*, (Ed.: A. R. Katritzky), Academic, San Diego, **2006**, pp. 1 – 108;.

[2] a) L. Antonov, V. Deneva, S. Simeonov, V. Kurteva, D. Nedeltcheva, J. Wirz, *Angew. Chem.* **2009**, *121*, 8015 – 8018; *Angew. Chem. Int. Ed.* **2009**, *48*, 7875 – 7878; b) S. Pu, Z. Tong, G. Liu, R. Wang, *J. Mater. Chem. C* **2013**, *1*, 4726 – 4739; c) G. Busseti, M. Campione, M. Riva, A. Picone, L. Rimondo, L. Ferraro, C. Hogan, M. Palummo, A. Brambilla, M. Finazzi, L. Duo, A. Sassella, F. Cicacci, *Adv. Mater.* **2014**, *26*, 958 – 963.

[3] W. Warr, *J. Comput. Aided Mol. Des.* **2010**, *24*, 497 – 520.

[4] a) A. R. Katritzky, C. D. Hall, B. E.-D. M. El-Gendy, B. Dragichi, *J. Comput. Aided Mol. Des.* **2010**, *24*, 475 – 484; b) P. Pospisil, P. Ballmer, L. Scapozza, G. Folkers, *J. Recept. Signal Transduction* **2003**, *23*, 361 – 371.

[5] a) F. H. Kamounah, L. Antonov, V. Petrov, G. J. van der Zwan, *J. Phys. Org. Chem.* **2007**, *20*, 313 – 320; b) D. L. Nedeltcheva, L. Antonov, *J. Phys. Org. Chem.* **2009**, *22*, 274 – 281; c) A. Afkhami, F. Khajavi, H. Khanmohammadi, *Anal. Chim. Acta* **2009**, *634*, 180 – 185; d) I. Sheikhshoaie, W. M. F. Fabian, *Curr. Org. Chem.* **2009**, *13*, 149 – 171.

[6] A. J. Cruz-Cabeza, C. R. Groom, *CrystEngComm* **2011**, *13*, 93 – 98.

[7] a) T. Steiner, G. Koellner, *Chem. Commun.* **1997**, 1207 – 1208; b) H. Pizzala, M. Carles, W. E. E. Stone, A. Thevand, *J. Mol. Struct.* **2000**, *526*, 261 – 268; c) B. D. Sharma, J. F. McConnell, *Acta Crystallogr.* **1965**, *19*, 797 – 806; d) F. Betchel, J. Gaultier, C. Hauw, *Cryst. Struct. Commun.* **1973**, *2*, 469 – 472.

[8] P. M. Bhatt, G. R. Desiraju, *Chem. Commun.* **2007**, 2057 – 2059.

[9] a) K. Užarević, M. Rubčić, V. Stilinović, B. Kaitner, M. Cindrić, *J. Mol. Struct.* **2010**, *984*, 232 – 239; b) W. Schilf, B. Kamiénski, K. Užarević, *J. Mol. Struct.* **2013**, *1031*, 211 – 215.

[10] a) C. Foces-Foces, A. L. Llamas-Saiz, R. M. Claramunt, C. Lopez, J. Elguero, *J. Chem. Soc. Chem. Commun.* **1994**, 1143 – 1145; b) P. Csomós, L. Fodor, A. Csampai, P. Sohar, *Tetrahedron* **2010**, *66*, 3207 – 3213; c) T. Holczbauer, L. Fabian, P. Csomos, L. Fodor, A. Kalman, *CrystEngComm* **2010**, *12*, 1712 – 1717; d) M. A. Garcia, C. Lopez, R. M. Claramunt, A. Kenz, M. Pierrot, J. Elguero, *Helv. Chim. Acta* **2002**, *85*, 2763 – 2776; e) A. Madinaveitia, E. Olay, *An. Soc. Esp. Fis. Quim.* **1933**, *31*, 134 – 138; f) F. Reviriego, I. Alkorta, J. Elguero, *J. Mol. Struct.* **2008**, *891*, 325 – 328; g) M. Bauer, R. K. Harris, R. C. Rao, D. C. Apperley, C. A. Rodger, *J. Chem. Soc. Perkin Trans. 2* **1998**, 475 – 481.

[11] A unique example of functional nonheterocyclic desmotrope: M. Rubčić, K. Užarević, I. Halasz, N. Bregović, M. Mališ, I. Đilović, Z. Kokan, R. S. Stein, R. E. Dinnebier, V. Tomišić, *Chem. Eur. J.* **2012**, *18*, 5620 – 5631.

[12] S. L. Price, *Chem. Soc. Rev.* **2014**, *43*, 2098 – 2111.

[13] K. Epa, C. B. Aakeröy, J. Desper, S. Rayat, K. L. Chandra, A. J. Cruz-Cabeza, *Chem. Commun.* **2013**, *49*, 7929 – 7931.

[14] A. Kálmán, *Acta Crystallogr.* **2005**, *B61*, 536 – 547.

[15] C. Wales, L. H. Thomas, C. C. Wilson, *CrystEngComm* **2012**, *14*, 7264 – 7274.

[16] M. R. Chierotti, L. Ferrero, N. Garino, R. Gobetto, L. Pellegrino, D. Braga, F. Grepioni, L. Maini, *Chem. Eur. J.* **2010**, *16*, 4347 – 4358.

[17] M. U. Schmidt, J. Bruening, J. Glinnemann, M. W. Huetzler, P. Moerschel, S. N. Ivashevskaya, J. van de Streek, D. Braga, L. Maini, M. R. Chierotti, R. Gobetto, *Angew. Chem.* **2011**, *123*, 8070 – 8072; *Angew. Chem. Int. Ed.* **2011**, *50*, 7924 – 7926.

[18] a) K. Užarević, M. Rubčić, I. Đilović, Z. Kokan, D. Matković-Čalogović, M. Cindrić, *Cryst. Growth Des.* **2009**, *9*, 5327 – 5333; b) K. Užarević, G. Pavlović, M. Cindrić, *Polyhedron* **2013**, *32*, 294 – 300.

[19] a) A. Blagus, D. Cinčić, T. Friščić, B. Kaitner, V. Stilinović, *Maced. J. Chem. Chem. Eng.* **2010**, *29*, 117 – 138.

[20] J. W. Ledbetter, Jr., *J. Phys. Chem.* **1968**, *72*, 4111 – 4115.

[21] a) T. Dziembowska, *Pol. J. Chem.* **1998**, *72*, 193 – 209; b) J. M. Fernandez-G, F. R. Portilla, B. Q. Garcia, R. A. Toscano, R. Salcedo, *J. Mol. Struct.* **2001**, *561*, 197 – 207; c) B. Kamieński, W. Schilf, T. Dziembowska, Z. Rozwadowski, A. Szady-Chełmieniecka, *Sol. St. Nucl. Magn. Res.* **2000**, *16*, 285 – 289.

[22] a) J. H. Day, *Chem. Rev.* **1963**, *65*, 65 – 80; b) J. H. Day, *Chem. Rev.* **1968**, *68*, 649 – 657; c) K. Nassau, *The Physics and Chemistry of Color*, 2nd ed. John Wiley and Sons, New York, **2001**.

[23] a) *Photochromism: Molecules and Systems*, (Eds.: H. Dürr, H. Bouas-Laurent), Elsevier, Amsterdam, **1990**, and references therein; b) J. R. Scheffer, R. P. Pokkuluri, in *Photochemistry in Organised and Constrained Media*, (Ed.: V. Ramamurthy), VCH Publishers, New York, **1990**, p. 185.

[24] K. Užarević, M. Rubčić, M. Radić, A. Puškarić, M. Cindrić, *CrystEngComm* **2011**, *13*, 4314 – 4323.

[25] a) I. Halasz, M. Rubčić, K. Užarević, I. Đilović, E. Meštrović, *New J. Chem.* **2011**, *35*, 24 – 27; b) T. Steiner, *Acta Crystallogr.* **2001**, *B57*, 103; c) T. R. Shattock, K. K. Arora, P. Vishweshwar, M. J. Zaworotko, *Cryst. Growth Des.* **2008**, *8*, 4533 – 4545; d) S. Mohamed, D. A. Tocher, M. Vickers, P. G. Karamertzanis, S. L. Price, *Cryst. Growth Des.* **2009**, *9*, 2881 – 2889.

[26] D. Lin-Vien, N. B. Colthup, W. G. Fateley, J. G. Grasselli, *The Handbook of Infrared and Raman Frequencies of Organic Molecules*, Academic Press, San Diego, **1991**.

[27] a) G. O. Dudek, G. P. Volpp, *J. Am. Chem. Soc.* **1963**, *85*, 2697 – 2702; b) P. Przybylski, W. Lewandowska, B. Brzezinski, F. Bartl, *J. Mol. Struct.* **2006**, *797*, 92 – 98.

[28] R. M. Issa, A. M. Khedr, H. Rizk, *J. Chin. Chem. Soc.* **2008**, *55*, 875 – 884.

[29] a) N. Galić, Z. Cimerman, V. Tomišić, *Anal. Chim. Acta* **1997**, *343*, 135 – 143; b) N. Galić, Z. Cimerman, V. Tomišić, *Spectrochim. Acta Part A* **2008**, *71*, 1274 – 1280; c) H. Ünver, M. Yıldız, N. Ocak, T. N. Durlu, *J. Chem. Crystallogr.* **2008**, *38*, 103 – 108.

[30] M. Ziołek, K. Filipczak, A. Maciejewski, *Chem. Phys. Lett.* **2008**, *464*, 181 – 186.

[31] a) G. P. Stahly, *Cryst. Growth Des.* **2007**, *7*, 1007 – 1026; b) K. Jarring, T. Larsson, B. Stensland, I. Ymén, *J. Pharm. Sci.* **2006**, *95*, 1144 – 1161.

[32] D. Cinčić, I. Brekalo, B. Kaitner, *Cryst. Growth Des.* **2012**, *12*, 44 – 48.

[33] P. Gans, A. Sabatini, A. Vacca, *Talanta* **1996**, *43*, 1739 – 1753.

[34] P. Gans, A. Sabatini, A. Vacca, *Annali di Chimica* **1999**, *89*, 45 – 49.

[35] Gaussian09, A.01. M. J. Frisch, G. W. Trucks, H. B. Schlegel, G. E. Scuseria, M. A. Robb, J. R. Cheeseman, G. Scalmani, V. Barone, B. Mennucci, G. A. Petersson, H. Nakatsuji, M. Caricato, X. Li, H. P. Hratchian, A. F. Izmaylov, J. Bloino, G. Zheng, J. L. Sonnenberg, M. Hada, M. Ehara, K. Toyota, R. Fukuda, J. Hasegawa, M. Ishida, T. Nakajima, Y. Honda, O. Kitao, H. Nakai, T. Vreven, J. A. Montgomery Jr., J. E. Peralta, F. Ogliaro, M. Bearpark, J. J. Heyd, E. Brothers, K. N. Kudin, V. N. Staroverov, R. Kobayashi, J. Normand, K. Raghavachari, A. Rendell, J. C. Burant, S. S. Iyengar, J. Tomasi, M. Cossi, N. Rega, J. M. Millam, M. Klene, J. E. Knox, J. B. Cross, V. Bakken, C. Adamo, J. Jaramillo, R. Gomperts, R. E. Stratmann, O. Yazyev, A. J. Austin, R. Cammi, C. Pomelli, J. W. Ochterski, R. L. Martin, K. Morokuma, V. G. Zakrzewski, G. A. Voth, P. Salvador, J. J. Dannenberg, S. Dapprich, A. D. Daniels, Ö. Farkas, J. B. Foresman, J. V. Ortiz, J. Cioslowski, D. J. Fox, Gaussian, Inc. Wallingford CT, **2009**.

[36] J.-D. Chai, M. Head-Gordon, *Phys. Chem. Chem. Phys.* **2008**, *10*, 6615 – 6620.

[37] R. Krishnan, J. S. Binkley, R. Seeger, J. Pople, *J. Chem. Phys.* **1980**, *72*, 650 – 654.
[38] G. Scalmani, M. J. Frisch, *J. Chem. Phys.* **2010**, *132*, 114110 – 114115.
[39] Oxford Diffraction, Oxford Diffraction Ltd., Xcalibur CCD system, CRYSALIS Software system, Version 1.170, **2003**.
[40] G. M. Sheldrick, SHELXS97, Program for the Solution of Crystal Structures, University of Göttingen, Germany, **1997**.
[41] G. M. Sheldrick, *Acta Crystallogr. Sect. A* **2008**, *64*, 112 – 122.
[42] L. J. Farrugia, *J. Appl. Crystallogr.* **1999**, *32*, 837 – 838.
[43] a) A. L. Spek, *Acta Crystallogr. Sect. A* **1990**, *46*, C34; b) A. L. Spek, PLATON, A Multipurpose Crystallographic Tool, Utrecht University, Utrecht, The Netherlands, **1998**.
[44] a) M. Nardelli, *Comput. Chem.* **1983**, *7*, 95 – 98; b) M. Nardelli, *J. Appl. Crystallogr.* **1995**, *28*, 659 – 673.

Received: May 15, 2014
Published online on ■■ ■■, 0000

FULL PAPER

Tautomerism

*M. Juribašić, N. Bregović, V. Stilinović, V. Tomišić, M. Cindrić, P. Šket, J. Plavec, M. Rubčić, K. Užarević**

■■ – ■■

Supramolecular Stabilization of Metastable Tautomers in Solution and the Solid State

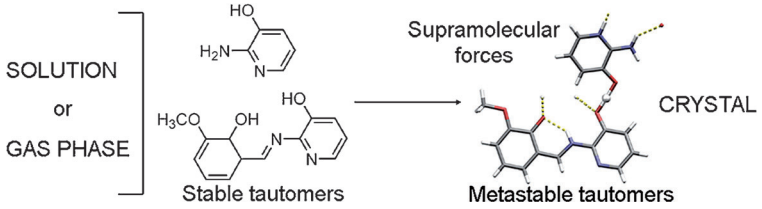

A stable relationship? The imine compound derived from 3-methoxysalicylaldehyde and 2-amino-3-hydroxypyridine crystallizes in three polymorphic forms, exclusively as a metastable keto–amino tautomer (see figure). Computations show that hydrogen bonding of the imine compound with suitable molecules shifts the tautomeric equilibrium to the less stable keto form, which was further used to obtain two metastable tautomers in multicomponent salts of the imine.